Available online at www.sciencedirect.com

jmr&t Journal of Materials Research and Technology

journal homepage: www.elsevier.com/locate/jmrt

Original Article

Improvement of high frequency giant magnetoimpedance effect in CoFeSiB amorphous ribbon with vanishing magnetostriction by electrodeposited Co coating surface layer

V. Vega [a], V.M. Prida [a,*], B. Hernando [a], M. Ipatov [b], A. Chizhik [b], V. Zhukova [b], A. Zhukov [b,c], L. Domínguez [d], J. González [b]

[a] Department of Physics, Faculty of Sciences, University of Oviedo, C/Federico García Lorca Nº 18, 33007, Oviedo, Spain

[b] Department of Advanced Polymers and Materials, Faculty of Chemistry, University of the Basque Country, Manuel de Lardizabal 3, 20018 San Sebastián, Spain

[c] IKERBASQUE Foundation, Bilbao, Spain

[d] Department of Applied Physics I, University of the Basque Country, Plaza Europa s/n, 20018, San Sebastián, Spain

ARTICLE INFO

Article history:
Received 9 October 2021
Accepted 26 November 2021
Available online 1 December 2021

Keywords:
Soft magnetic amorphous ribbon
Coating layer
Electrodeposition
Giant magnetoimpedance effect
Magnetic anisotropy
Magneto-optical kerr effect

ABSTRACT

The influence of a ferromagnetic cover layer on giant magnetoimpedance (GMI) effect in nearly-zero magnetostrictive $Co_{66.5}Fe_{3.5}Si_{12.0}B_{18.0}$ amorphous ribbon after being surface coated by an electrodeposited Co layer of 10 μm in thickness, has been studied in the high frequency range between 10 MHz and 1.5 GHz. Longitudinal MOKE measurements performed on both kind of samples reveal the influence of exchange coupling interaction at the interface between the magnetic amorphous ribbon and electrodeposited Co coating layer, which is sensitive to the skin depth effect at high ac current frequency values. Comparison between GMI responses of the Co coated amorphous ribbon and the as-cast sample is provided. A more sharp and well defined double-peaks dependence of impedance on magnetic field, but with lower peaks intensity, is observed for the Co coated ribbon in the frequency range of 10–100 MHz, while the peaks intensity is higher than that observed in the as-cast ribbon at the high frequency value of 1 GHz due to the higher resistance of the Co electroplated layer than the core one. The influence of a *dc* bias drive current on the GMI response in both amorphous ribbons (as-cast and Co layered) is analyzed, which originates the removal of magnetic domain structure from both, the as-cast and Co-coated ribbons, giving rise more sensitive GMI effect. CoFeSiB amorphous ribbon with vanishing magnetostriction can achieve improved high frequency magnetic properties after being surface coated with electrodeposited ferromagnetic layers, as outstanding candidates for electromagnetic and magnetomechanical engineering applications.

* Corresponding author.
E-mail address: vmpp@uniovi.es (V.M. Prida).

https://doi.org/10.1016/j.jmrt.2021.11.143

1. Introduction

The giant magnetoimpedance (GMI) effect discovered in 90-s in magnetically soft amorphous wires with vanishing magnetostriction [1,2] has attracted since then substantial interest owing principally to extremely large magnetic field sensitivity (up to 10%/A/m) suitable for real technological applications in magnetic sensors [3–8]. The origin of GMI effect is intrinsically related to the magnetic softness of the ferromagnetic conductor material [1–4]. Therefore, the GMI effect has been reported in a vast number of soft magnetic materials, including various families of magnetic wires [1–5,7–10], amorphous and nanocrystalline ribbons [4,6,11–15], multilayers [16–19] or lanthanide compounds [20,21]. Accordingly, the GMI effect optimization is greatly affected by advances in research on soft magnetic materials. Main research on GMI materials is therefore focused on influence of microstructure (amorphous, nanocrystalline or mixed structures), tuning of magnetic anisotropy through shape and magnetoelastic anisotropies [4,5,9,11,12]. Consequently, the development of GMI materials is multidisciplinary research involving materials science, micromagnetics and classical electrodynamics (see in particular Refs. [4,22,23]).

The GMI effect consists in a large change in the electrical impedance, Z, upon the applied magnetic field, H [1–5,23]. The origin and main features of GMI effect have been satisfactorily explained in terms of classical electrodynamics, by considering the skin effect of a soft magnetic conductor [1,2,4,5,23].

The peculiar magnetic domain structure exhibited by low magnetostrictive Co-rich wires, consisting of an axially magnetized inner core and the outer domain shell with high circumferential permeability (10^4) is sensitive to an axially applied external magnetic field [4,23,24], or tensile and torsional stresses [10,25–28]. Therefore, such materials usually present high GMI effect [1–5,23]. On the other hand, the shape magnetic anisotropy (cylindrical or planar geometry), sample dimensions (diameters, thickness) and the character and spatial magnetic anisotropy distribution (longitudinal or transverse) lead to remarkable differences in the GMI effect value and magnetic field dependence [4,23]. Thus, the $Z(H)$ dependence is determined by the type of magnetic anisotropy: the frequency range, single or double-peak $Z(H)$ dependence [29]. Consequently, considerable efforts have been devoted to modifying the magnetic domain structure in the surface layer of GMI materials in order to tune the GMI effect magnitude and the $Z(H)$ dependence [9,22,30–32].

As mentioned above, GMI effect has been also studied in thin films and even in sandwich structure [16–19,31,33–35]. One of factors relevant for the GMI effect optimization in thin films and magnetic microwires is the frequency of the AC driving current [36]. For amorphous ribbons or wires the optimal frequency range at which maximum change of impedance can be achieved is usually of the order of MHz [37,38]. However, in thin films and microwires the maximum of GMI effect is observed in the frequency range of around 100 MHz [16–19,22,36,39]. Accordingly, a decrease in the dimensionality of modern magnetic materials is associated with an increase in the optimal frequency range of GMI response [16–19,22,36,39].

However, given some specific applications for GMI effect in highly sensitive integrated micromachined magnetic sensors. (e.g. in the automotive sector, where high frequency noise can affect engine control computers), it is desirable to reduce operating frequencies but without reducing the GMI response [40,41].

One of the promising solutions involves targeted surface magnetic structure modification of amorphous or nanocrystalline soft magnetic materials using a magnetic thin film coating [42–44]. Focusing the attention on the advance to understand the fundamental mechanisms of the GMI effect, the improvement of high frequency GMI response and modification of optimal frequency have been achieved by either using of a magnetic Co thin film layer coating to an amorphous Co-based, Finemet or FeNi-based nanocrystalline ribbons [42–45].

The influence of electrodeposited cobalt and nickel layers with varying thicknesses ranging between 5 and 40 nm on the magnetoimpedance response of a soft ferromagnetic Co-based amorphous ribbon has been reported by L Jamilpanah et al. [46]. The higher crystallinity exhibited by Ni-deposited layers and the amorphous ferromagnetic nature of Co-deposited ones explain the different high frequency MI behaviour between the Co-deposited ribbons, which showed MI hysteretic behavior with an optimum response for the cover layer of 20 nm in thickness, and the non-hysteretic MI effect in Ni-deposited ribbons. The origin of this peculiar MI response is due to the exchange coupling effect occurred at the interface between the magnetic bilayers that is sensitive to the skin effect at high frecuency values of *ac* current. The GMI response is enhanced in these Ni- and Co-deposited ribbons at low thickness of deposited layers regarding to bare Co-based amorphous ribbon, but the increase of electrodeposited Co and Ni thickness layer makes to decrease significantly the MI effect.

Additive fabrication procedure by combining one-step electroless-plating for the synthesis of reduced graphene oxide (rGO) layer on Finemet ribbons, together magnetron sputtering method for the deposition of an FeCo coating layer, was followed for obtaining a peculiar sandwich structure made of Finemet/rGO/FeCo composite ribbon exhibiting high GMI effect values up to 70%, which are larger than in bare Finemet ribbon [47].

High sensitive magnetoimpedance effect, and good corrosion stability in aggressive environments, are functional properties exhibited by Co-rich amorphous ribbons-based sensitive elements that can be modified by deposition of magnetic and non-ferromagnetic layers with required conductivity, for magnetic biosensors applications. In this regard, bilayered $Fe_{20}Ni_{80}/Co_{67}Fe_3Cr_3Si_{15}B_{12}/Fe_{20}Ni_{80}$ magnetic composites were obtained by magnetron sputtering deposition of 1 μm thick conductive $Fe_{20}Ni_{80}$ films coated onto both sides of ferromagnetic Co-based amorphous ribbon, aimed for designing MI biosensors for magnetic label detection [48].

In spite of promising results, obtained in magnetic thin film coated Finemet or FeNi-based nanocrystalline ribbons, amorphous materials usually present enhanced mechanical properties [49]. Additionally, vanishing magnetostriction, λ_s,

values can also be obtained in Co-rich Co–Fe amorphous alloys, which determine the outstanding GMI behaviour exhibited by these materials [50,51].

Previously, we have studied the GMI effect in the as-cast and stress-annealed $Co_{66.5}Fe_{3.5}Si_{12.0}B_{18.0}$ amorphous ribbons [52–54]. In these previous works, we paid attention on correlation of the transverse magnetic anisotropy distribution through the cross section and the *Z(H)* dependencies (GMI effect magnitude, magnetic field value associated to the appearance of the two-peaks behaviour). Particularly, we showed that the GMI effect of stress-annealed ribbons was improved (GMI effect value as well as the narrower and sharper peaks in *Z(H)* dependencies) as compared to the as-cast ribbon. Such positive impact of stress-annealing induced anisotropy can be attributed to the development of a higher transverse magnetic susceptibility after stress-annealing treatment [53,55–57]. These findings become also relevant for the future high performance GMI-based technological and biomedical applications of amorphous materials [58–61].

The evolution of the maximum on *Z(H)* dependencies, attributed to the magnetic anisotropy field, as a function of the frequency can provide useful information on the spatial distribution of magnetic anisotropy of the ribbons. On the other hand, it is well known that electrochemical deposition technique is a suitable and low-cost method for making uniform metallic coatings on the surface of conductive substrates, such as soft magnetic amorphous ribbons, which allows also to properly modify the high frequency response of the magnetic materials [42–48], among other several deposition techniques [62–64].

Consequently, in this paper we provide our recent results on the GMI effect in near-zero magnetostriction Co-based amorphous ribbons coated with an electrochemical deposited Co layer, allowing to tailor the GMI effect in both, either intensity as well as in shape, for the high frequency range up to 1.5 GHz. The influence of an externally applied DC bias field is also analyzed.

2. Experimental details

Amorphous $Co_{66.5}Fe_{3.5}Si_{12.0}B_{18.0}$ (nominal composition) ribbons (0.60 mm of width and around 23 μm thick) were prepared employing the melt-spinning technique using a Fe wheel. The ribbons were rapidly quenched from the melt in a 10^{-3} mbar vacuum, (in the following it will be denoted as the as-cast sample). Examination of the as-cast sample revealed that it was amorphous with saturation magnetization, M_S, of about $M_S = 0.59$ T and the saturation magnetostriction, λ_S, (measured by the small angle magnetization rotation (SAMR) method of $\lambda_S = -0.22 \times 10^{-6}$. To mention that small value of saturation magnetostriction is a pre-requisite to exhibit large GMI effect in the soft magnetic amorphous alloys [23]. A piece of the as-cast ribbon, of around 2 cm in length, was coated with a different magnetic material in order to tune its magnetoimpedance response (denoted as Co-coated sample). A uniform Co layer was deposited on the surface of the as-cast ribbon by electrochemical deposition, performed in a Watts type electrolyte containing 300 g/l of $CoSO_4.7H_2O$, 45 g/l of $CoCl_2.6H_2O$ and 45 g/l of boric acid, with pH around 4.5 adjusted by dropping 3 M NaOH solution. The electrolyte was kept at 35 °C during the deposition process. The electrodeposition was performed in a three-electrode electrochemical cell, equipped with a saturated KCl Ag/AgCl reference electrode, a platinum wire as the counter electrode, and the ribbon acting as cathode. The applied deposition potential was −1 V vs. reference electrode, and it was kept during 300 s. The chemical composition and microstructure of both, the as-cast and cobalt coated samples were studied by Scanning Electron Microscopy (SEM JEOL-6610LV) equipped with Energy Dispersive X-ray analysis (EDX). Magnetic hysteresis loops, *M(H)*, of bulk samples (with different configurations of the applied magnetic field) have been measured at 300 K using a Vibrating Sample Magnetometer (VSM-VersaLab, QD) at applied magnetic fields up to 2.4×10^3 kA/m. Local surface magnetic properties were measured at room temperature (RT) by longitudinal Magneto-Optical Kerr Effect (LMOKE) carried out in a NanoMOKE3 device (Durham Magneto-Optics), suited with a dipolar electromagnet under a maximum applied field range of ±96 kA/m that was applied along both, the longitudinal or transversal directions with respect to the ribbon rolling direction.

The electrical impedance, Z, dependence on magnetic field, H, (up to 15 kA/m) applied along the longitudinal direction of 1 cm long ribbon was measured using a N5230A vector network analyzer at frequencies, *f*, up to 1.5 GHz, such as previously described elsewhere [52]. Z values were evaluated from reflection coefficients measurements. The N5230A vector network analyzer output power was −10 dBm.

3. Results and discussion

SEM images of the fracture cross-section and the ribbon surface for the as-cast ribbon and the Co-coated sample are shown in Fig. 1a and (b), respectively. The examination of the as-cast sample shows the typical morphology for an amorphous ribbon without traces of crystalline grains resulting from the quenching process.

The cross-section in Fig. 1b for the Co-coated sample clearly displays a Co layer of 10 μm revealing a laminar structure induced by the electrochemical deposition process. EDX microanalysis was performed in different ribbon zones including the Co layer for the chemical composition analysis. Both ribbons exhibit an average composition rather near to the nominal one, and no diffusion from Co layer to the ribbon sample has been observed. The estimated error determined for the concentration of each element was ±0.1%.

Accordingly, both ribbon and Co-coating thickness and chemical compositions are rather homogeneous and reproducible.

To assess the effect of Co coating layer on the magnetic properties of the amorphous ribbon, we measured the magnetic hysteresis loops of the Co-coated sample along the longitudinal, transversal in-plane and perpendicular applied magnetic field directions with respect to the ribbon axis (corresponding hysteresis loops of the as-cast sample were published in [54]). Figure 2 shows the normalized *M(H)* curves of the Co-coated sample. The coercivity and anisotropy field

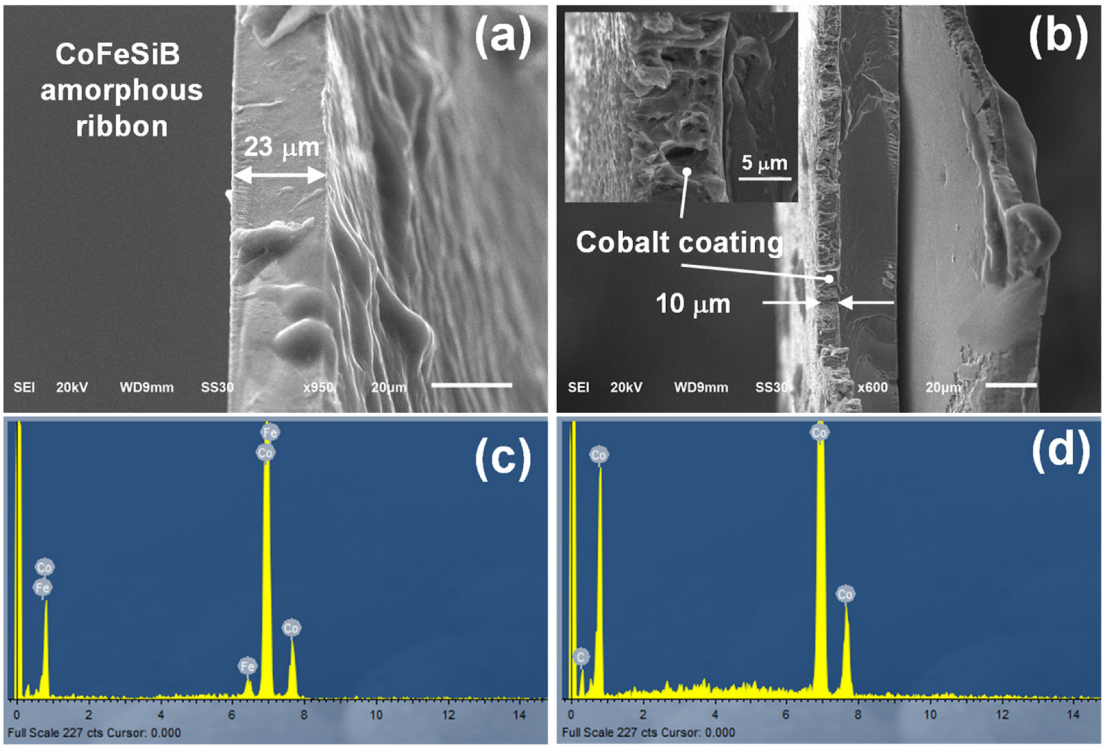

Fig. 1 – (a) and (b) SEM images of the cross section of the as-cast $Co_{66.5}Fe_{3.5}Si_{12.0}B_{18.0}$ ribbon (a), and Co-coated amorphous ribbon (b). The inset in (b) displays a higher magnification image of the cobalt coating, evidencing its laminar structure. (c) and (d) display the EDX spectra obtained from the as-cast ribbon (c), and the Co coating layer (d), respectively.

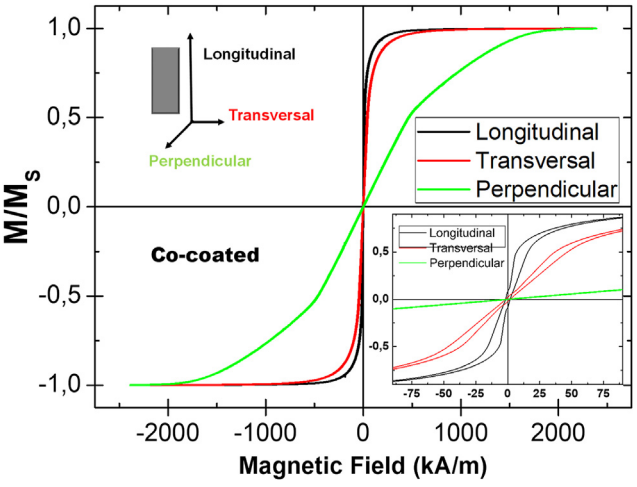

Fig. 2 – Room temperature magnetic hysteresis loops measured along the in-plane ribbon axis (black), transversal direction in the ribbon plane (red) and perpendicularly applied external field to the ribbon plane (green) of Co-coated $Co_{66.5}Fe_{3.5}Si_{12.0}B_{18.0}$ amorphous ribbon. The inset shows a magnification at low field values.

values that were extracted from the hysteresis loops of both samples are shown in Table I.

It was previously reported that the as-cast ribbon is magnetically soft with almost rectangular longitudinal hysteresis loop and with the magnetization reached the saturation achieved at low H-values. However, the transversal and perpendicular hysteresis loops were inclined. This shape of these hysteresis loops has been explained considering a peculiar magnetic domain structure with mainly two regions: an inner axially magnetized core responsible of the low field hysteresis and the outer shell with the transverse magnetization orientation with respect to the ribbon axis, linked to transversal magnetic anisotropy and responsible for the *M(H)* inclination.

Table 1 – Coercivity (H_C) and effective anisotropy field (H_K) values obtained from longitudinal, transversal and perpendicular VSM bulk hysteresis loops of the as-cast and Co-coated ribbons, respectively. (Data of the uncoated ribbon were obtained from the hysteresis loops published in [52]).

CoFeSiB Ribbon	$H_{C\ long}$ (kA/m)	$H_{C\ trans}$ (kA/m)	$H_{C\ perp}$ (kA/m)	$H_{K\ long}$ (kA/m)	$H_{K\ trans}$ (kA/m)	$H_{K\ perp}$ (kA/m)
as-cast	0.48	0.48	0.48	6.0	49.2	646.4
Co-coated	1.84	1.84	2.88	528.0	696.0	1920.0

The origin of this transversal magnetic anisotropy has been discussed in terms of two main sources: magnetoelastic and the shape anisotropies. Obviously, the former plays an important role in obtaining the transverse component of the magnetic permeability, which is very sensitive to the applied magnetic field, for the GMI effect observation. The anisotropy field, H_K, magnitude, evaluated from the transversal hysteresis loops can be one order of magnitude larger than that deduced from the $Z(H,f)$ dependencies (see discussion below). This discrepancy can be explained by a strong demagnetizing effect in the transverse direction. It is worth noting that the coercivity (H_C) value remains unchanged regardless the magnetic field direction due to the amorphous structure of the as-cast sample, but the change in the H_k is noticeable, being larger for the $M(H)$ curves along the perpendicular direction to the ribbon plane owing to the highest demagnetizing factor.

Relative to their uncoated counterparts, the Co-coated sample exhibits an enhancement in both coercivity and anisotropy field. H_C remains unchanged when is measured along the longitudinal and transversal directions. However, an increase in H_C is observed for the Co-coated ribbon, when the hysteresis loop is measured perpendicularly to the ribbon plane, likely associated with the transition from the amorphous to polycrystalline structure of the Co layer. The same feature should be responsible for the enhancement of the anisotropy field, H_K. The coexistence of the polycrystalline structure and the amorphous matrix in this sample, and the corresponding arrangement of their respective anisotropies, result in an easy magnetization direction deviating at a certain angle from the ribbon axis. This fact is a favourable condition to observe the double-peak behavior of GMI effect.

In contrast to VSM measurements, which are providing information about the magnetic behavior of the whole bulk ribbon, thus including the contribution of both, the amorphous matrix and the polycrystalline cobalt coating layer, LMOKE characterization is sensitive to the surface magnetic properties in both samples, as it is displayed in Fig. 3.

In the as-cast sample, shown in Fig. 3 a) for the magnetic field applied along the rolling direction of the ribbon, the LMOKE measurement evidences the soft magnetic properties of the amorphous ribbon that exhibits a more bistable magnetic behavior, in good agreement with VSM measurements. However, the LMOKE hysteresis loop of the Co-coated sample shown in Fig. 3 c) displays larger values of coercivity (~8 kA/m) and higher saturation field (~50 kA/m), which are associated to the hard magnetic features of the electrodeposited cobalt coating layer.

Turning the applied magnetic field towards the in-plane transversal direction respect to the rolling axis of the ribbon, it can be seen in the Fig. 3 b) that the LMOKE hysteresis loop of

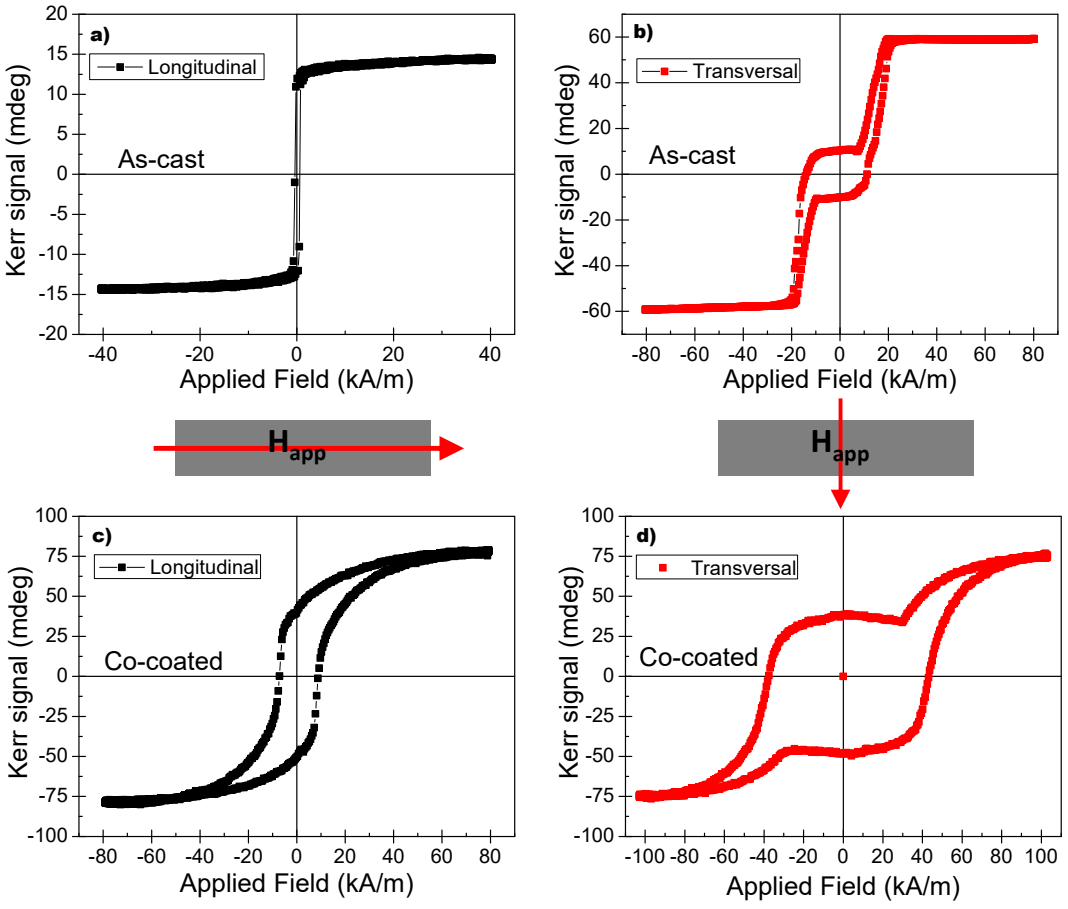

Fig. 3 – Longitudinal MOKE hysteresis loops measured at room temperature for: a) as-cast and c) Co-coated CoFeSiB ribbons for magnetic field applied along the in-plane ribbon axis; b) as-cast and d) Co-coated CoFeSiB ribbons, when the magnetic field is applied transversal to the ribbon axis.

the as-cast sample displays a complex magnetic behavior characterized by superposition of a square loop at relatively low field values (~12 kA/m), and tilted magnetization branches until the saturation of magnetization is reached at the higher field value of around 20 kA/m. This complex magnetic behavior can be ascribed to the existence of a certain transversal magnetic anisotropy induced in the ribbon, which is usual for very low magnetostrictive amorphous ribbons, in combination with an axially magnetized core, as previously discussed for VSM measurements.

It is worth to note that, this complex magnetic behavior still appears in the LMOKE hysteresis loop of the Co-coated sample displayed in the Fig. 3 d), which is accompanied also by an increase in coercivity (~40 kA/m) and magnetization saturation field (~80 kA/m) that can be associated to the polycrystalline structure of the electrodeposited Co coating layer. Therefore, and considering the fact that LMOKE technique is mainly sensitive to the surface magnetic properties of the sample, these experimental measurements suggest that the magnetization dynamics of the amorphous ribbon plays an important role on the magnetic behavior of the external Co layer, being both layers magnetically exchange coupled.

In order to elucidate the Co coating impact on the GMI effect, magnetic field and frequency dependences of impedance, Z, of the 10 μm thickness Co-coated ribbon sample were studied systematically. Similar results of GMI obtained in the uncoated as-cast sample were published previously in [54]. Figure 4 shows the 3D *Z(H,f)* dependencies of the Co-coated sample, in which we can observe two symmetrical peaks on *Z(H)* dependencies for each *f*-value. Additionally, the two-peaks *Z(H)* dependencies emerges more clearly with *f* increasing.

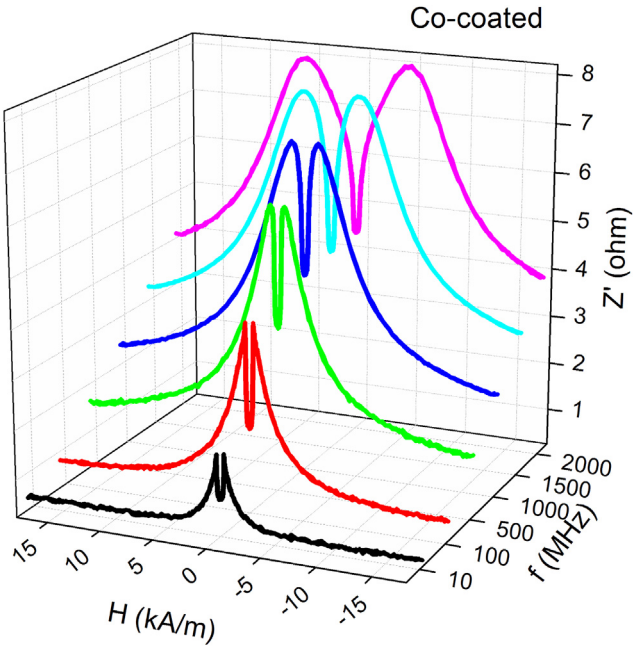

Fig. 4 – Impedance of the Co-coated sample as a function of the magnetic field applied along the ribbon longitudinal axis, for different frequency values in the range between 10 MHz and 1.5 GHz.

As discussed above, the *H*-value corresponding the *Z* maximum values (to the peaks on *Z(H)* dependencies) is linked to the average magnetic anisotropy field, H_K, value in 100 MHz frequency range (but for $f < 1$ GHz). Moreover, the shape of *Z(H)* dependencies, in same way, reflects the magnetic anisotropy distribution in the sample [53,58,65].

As expected from previous publications on the frequency dependence of the GMI effect [22,66], an increase in the *H*-values corresponding to the maximum of Z with frequency increasing is observed, while the two-peak character of the *Z(H)* dependences remains (see Fig. 4).

The evolution of *Z(H)* dependencies with the AC current frequency, *f*, can be explained by considering the frequency dependence of the skin penetration depth, δ, given for the case of a magnetic ribbon by [4,11,42–48,50,52–58]:

$$\delta = (\pi \sigma \mu_t \, f)^{-1/2} \quad (1)$$

where σ is the electrical conductivity and μ_t is the transversal magnetic permeability.

Accordingly, upon *f* increasing, a decrease in δ is produced and a permeability modification is expected. However, when a sufficiently high longitudinal magnetic field is applied, magnetic saturation is achieved, giving rise to a decrease in the transverse magnetic permeability. Therefore, an increase in δ and a decrease in *Z* are observed.

It is worth mentioning that at GHz frequency range the GMI peaks are shifted into *H* range at which the sample is magnetically saturated, i.e. larger than H_K. In this *f* range, the *Z(H)* dependencies have been attributed to the ferromagnetic resonance (FMR) [36,67,68].

The GMI response in this Co-coated sample results to be very similar to that published for the as-cast ribbon. Nevertheless, the spread of the GMI peaks in the Co-coated sample is more significant as compared to the uncoated sample. This difference must be attributed to the presence of a Co layer, which enhances the dispersion of the transverse magnetic anisotropy, since the coating of the sample surface has caused some stress, as can be deduced from the hysteresis loops shown in the Figs. 2 and 3. Additionally, the chemical composition and hence the magnetic anisotropy distribution in the surface layer of the Co-coated sample is different to the as-cast ribbon.

Noticeably, the impact of the Co-coating on the GMI ratio reported in [44] for an FeNi-based nanocrystalline ribbon was quite similar to the here reported in this work. The enhancement of the GMI peak shape after the sample coating promotes the use of magnetic coatings to improve the performance of GMI-based sensors [44–48].

The evolution of the anisotropy field, H_K, with the frequency, *f*, of the Co-coated sample is shown in the Fig. 5, where H_K is the magnetic field value corresponding to the *Z* maximum for the sample coated with the Co layer. It is logical that with the frequency increasing, the penetration depth, δ, decreases, and the current flows through the thinner surface layer of the sample. The H_K -values obtained from Fig. 4, should be attributed to a thin surface layer of the sample. The thickness of this surface layer (different for each frequency), in which the current flows, strongly depends on the stresses distribution and on the composition in the surface region,

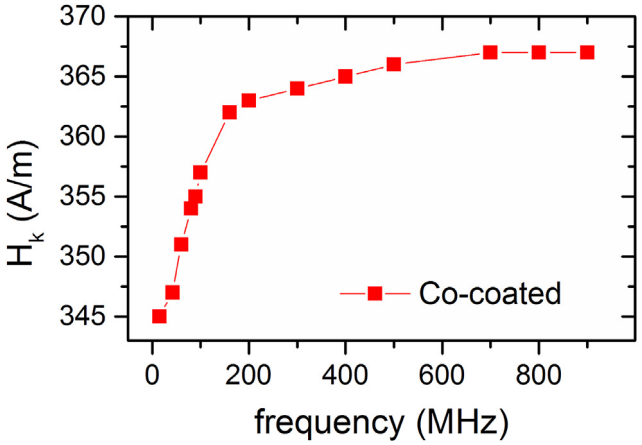

Fig. 5 – Frequency dependence of the anisotropy field for the Co-coated ribbon. Anisotropy field corresponds to the value of applied magnetic field at the maximum GMI ratio for each frequency.

which is directly related to the skin effect in a ferromagnetic conductor. As the frequency of the AC current increases, one should expect a decrease in the effective thickness of the surface area (see Eq. (1)), and it is reasonable to assume a substantial change in the transverse magnetic permeability of the effective surface area where the AC current flows across it. Therefore, it is reasonable to assume that a decrease in effective thickness of surface area due to skin effect significantly affects the GMI response.

It must be noted that the increase of H_K with f in this Co-coated ribbon is quite different to that observed in the uncoated as-cast ribbon reported in [54], where a dependence of $H_K = a+bf^n$ was obtained (the parameter a represents the anisotropy field at $f = 0$ Hz, being in good agreement with the H_K value deduced from the DC hysteresis loop). Nevertheless, the frequency, f, dependence of H_K in the Co-coated ribbon (Fig. 5) does not follow the abovementioned relationship. It can be seen like two regions, being the frequency of around 200 MHz that defines the two regions indicating different state of mechanical internal stresses owing to the presence of the Co layer to modify the magnetoelastic anisotropy across the surface region. Even, the saturation magnetostriction is also sensing the changes of internal stresses in this nearly-zero magnetostrictive amorphous ribbon [69,70].

For deeper information on the GMI behavior, we analyzed low field regions of the $Z(H)$ dependencies in both samples (see Fig. 6). Ripples in the $Z(H)$ dependences at a low frequency (10 MHz) in both samples (see Fig. 6a) may indicate an irregular magnetic domains structure. At a higher frequency (100 MHz) (Fig. 6b), the Z(H) dependence becomes somewhat stable. The as-cast ribbon exhibits higher GMI effect than the Co-coated sample. It is more pronounced in the as-cast ribbon, that is, more intensive regarding the maximum value, although the peaks are sharper in the Co-coated sample, which is an advantage for future applications based on the GMI effect.

At 1 GHz (Fig. 6, c), the $Z(H)$ dependence becomes quite stable because almost no ripple is observed. At a high frequency, the penetration depth, δ, decreases and the current is

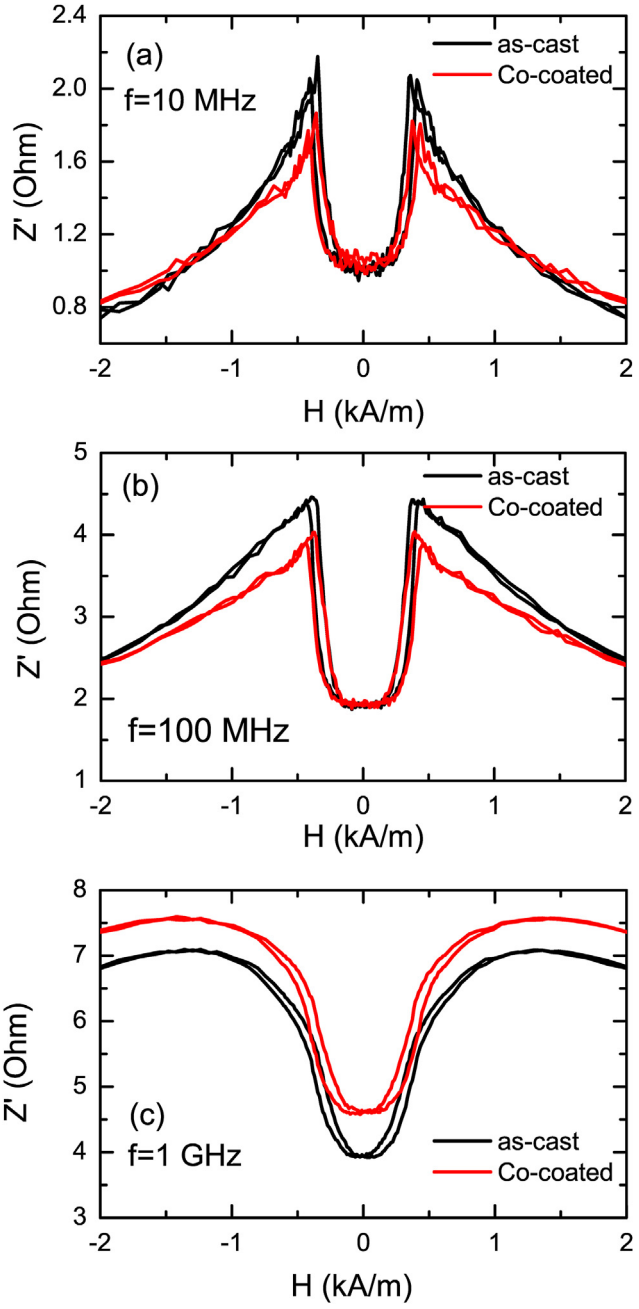

Fig. 6 – Impedance dependence with the applied magnetic field of the as-cast and Co-coated ribbons at different drive current frequency: (a) 10 MHz; (b) 100 MHz; and (c) 1 GHz.

concentrated on the ribbons surface where the magnetic domain structure is probably more regular. One can note that the GMI dependence of Co-coated sample is shifted up, which could mean that the Co electroplated layer exhibits a higher resistance than the core one. The GMI hysteresis suggests the existence of a complex magnetic domain structure and core–shell interaction [71,72].

Further, we have studied the influence of the DC bias current, I_B, on the electrical impedance for the Co-coated ribbon, as it is shown in Fig. 7.

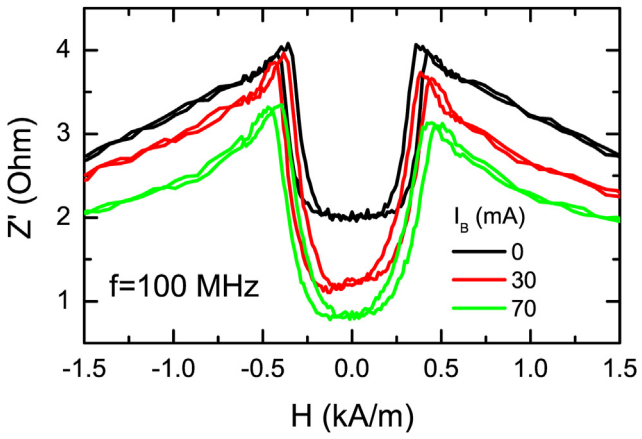

Fig. 7 – Impedance response of the Co-coated ribbon as a function of the applied magnetic field at 100 MHz measured at different values of the DC drive bias current (I_B = 0, 30 and 70 mA).

As one can see, $Z(H)$ is also sensitive to I_B in the Co-coated sample, in a similar way to displayed for the as-cast ribbon [54]. The *DC* bias current, I_B, creates a static transverse and inhomogeneous magnetic field, H_B, which rotates the magnetization vector giving rise to the impedance change of the Co-coated ribbon. The application of I_B results in the decreasing of impedance, thus for $H = 0$ the impedance is 2 Ohm at $I_B = 0$ and decreases more than twice when I_B of 70 mA is applied. The decrease in the impedance and the increase of GMI ratio ($\Delta Z/Z = [Z(H) - Z(H_{max})]/Z(H_{max})$) is probably related with removing of the magnetic domain structure and domain wall from the regions exhibiting a high impedance and lower GMI effect [65]. We also noted that in ribbons a considerable higher bias current is required to eliminate the magnetic domain structure than in amorphous glass-coated microwires, which is of the order of a few milliamperes [73,74].

4. Conclusions

Concluding, the impact of the Co coating (layer with 10 μm in thickness) on the magnetic properties and high frequency impedance of the $Co_{66.5}Fe_{3.5}Si_{12.0}B_{18.0}$ amorphous ribbon has been studied. Such research is directed towards the development of novel materials with improved GMI effect, such as the case of Co-coated amorphous ribbon. An experimental study of the GMI response in the high frequency range (from a few MHz up to GHz) was carried out in two kinds of ribbons (coated and uncoated). The high frequency GMI measurements provide rather similar response values in both samples. Nevertheless, thinking on future applications to note that, as a sign of quality the spread of the GMI peaks of the Co-coated ribbon results to be more significant as comparing with the ones for the as-cast ribbon. Thus, the frequency dependence of magnetic anisotropy field in this Co-coated ribbon is quite different to that observed in the uncoated ribbon. Such modification has been discussed considering different state of mechanical internal stresses owing to the presence of the surface Co layer. Comparative studies of hysteresis loops provided by the VSM and LMOKE techniques measurements, allows to elucidate the contribution of both magnetically coupled layers from the amorphous matrix and the polycrystalline electrodeposited Co coating layer.

Another important implication of this study is that we have demonstrated that an additional ferromagnetic metal coating layer can be used to tune and optimize the GMI response of magnetically soft amorphous ribbon by controlling the composition and thickness of this surface magnetic coating layer, and that electrochemical deposition is a suitable method for this technical purpose.

Declaration of Competing Interest

The authors declare that they have no known competing financial interests or personal relationships that could have appeared to influence the work reported in this paper.

Acknowledgments

This work was supported by the Spanish MCIU, under PGC2018-099530-B-C31 (MCIU/AEI/FEDER, UE), by the Government of the Basque Country, under PIBA 2018–44, PUE_2021_1_0009 and Elkartek (CEMAP and AVANSITE) projects, and by the University of the Basque Country, under the scheme of "Ayuda a Grupos Consolidados" (Ref.: GIU18/192) and COLAB 20/15 project. This research was also partially funded by Spanish Ministerio de Ciencia e Innovación (MICINN) and Research Agency State (AEI), under grant number PID2019-108075RB-C32. The authors are thankful for the technical and human support provided by SGIker of UPV/EHU (Medidas Magnéticas Gipuzkoa) and European funding (ERDF and ESF). Scientific support of Common Research Services (SCTs) from University of Oviedo is also acknowledged.

REFERENCES

[1] Panina LV, Mohri K. Magnetoimpedance effect in amorphous wire. Appl Phys Lett 1994;65:1189–11191. https://doi.org/10.1063/1.112104.
[2] Beach RS, Berkowitz AE. Giant magnetic field dependent impedance of amorphous FeCoSiB wire. Appl Phys Lett 1994;64:3652–4. https://doi.org/10.1063/1.111170.
[3] Zhukova V, Chizhik A, Zhukov A, Torcunov A, Larin V, González J. Optimization of giant magnetoimpedance in Co-rich amorphous microwires. IEEE Trans Magn 2002;38:3090. https://doi.org/10.1109/TMAG.2002.802397.
[4] Phan M-H, Peng H-X. Giant magnetoimpedance materials: fundamentals and applications. Prog Mater Sci 2008;53:323–420. https://doi.org/10.1016/j.pmatsci.2007.05.003.
[5] Zhukov A, Ipatov M, Zhukova V. Advances in giant magnetoimpedance of materials. In: Buschow KHJ, editor. Handbook of magnetic materials, vol. 24; 2015. p. 139–236. https://doi.org/10.1016/BS.HMM.2015.09.001 [chapter 2].
[6] Vázquez M, Badini G, Pirota K, Torrejón J, Zhukov A, Torcunov A, et al. Applications of amorphous microwires in

sensing technologies. Int J Appl Electromagn Mech 2007;25(1–4):441–6. https://doi.org/10.3233/JAE-2007-744.
[7] Yang Z, Lei C, Zhou Y, Liu Y, Sun XC. A GMI biochip platform based on Co-based amorphous ribbon for the detection of magnetic Dynabeads. Anal. Methods 2015;7:6883–9. https://doi.org/10.1039/C5AY01498K.
[8] Chen J, Li J, Xu L. Highly integrated MEMS magnetic sensor based on GMI effect of amorphous wire. Micromachines 2019;10:237. https://doi.org/10.3390/mi10040237.
[9] Zhukova V, Corte-León P, Ipatov M, Talaat A, Blanco JM, Olivera J, et al. Tailoring of magnetic softness and GMI effect in Fe-rich thin magnetic wires. AIP Adv 2018;8:056102. https://doi.org/10.1063/1.5004701.
[10] Liu J, Pang M, Cao G, Qu G, Wang X, Zhang Y, et al. Comparative study of tensile properties and magnetic properties for Nb-doped Fe-based wires. J. Mater. Res. Technol. 2020;9(6):12907–16. https://doi.org/10.1016/j.jmrt.2020.09.004.
[11] Hernando B, Sánchez ML, Prida VM, Tejedor M, Vázquez M. Magnetoimpedance effect in amorphous and nanocrystalline ribbons. J Appl Phys 2001;90:4783. https://doi.org/10.1063/1.1408594.
[12] Prida VM, Gorria P, Kurlyandskaya GV, Sanchez ML, Hernando B, Tejedor M. Magneto-impedance effect in nanostructured soft ferromagnetic alloys. Nanotechnology 2003;14:231. https://doi.org/10.1088/0957-4484/14/2/325.
[13] Corte-León P, Zhukova V, Domínguez L, Blanco JM, Ipatov M, Chizhik A, et al. Giant magnetoimpedance optical Kerr effects in $(Co_{63}Ni_{37})_{75}Si_{15}B_{10}$ amorphous ribbon. Intermetallics 2020;125:106925. https://doi.org/10.1016/j.intermet.2020.106925.
[14] Pan P, Moorehead RD, Hayward TJ. Influence of geometry on the giant magnetoimpedance of high-aspect ratio amorphous magnetic ribbons. J Appl Phys 2020;128:174504. https://doi.org/10.1063/5.0022777.
[15] Arzuza LCC, Béron F, Pirota KR. High-frequency GMI hysteresis effect analysis by first-order reversal curve (FORC) method. J Magn Magn Mater 2021;534:168008. https://doi.org/10.1016/j.jmmm.2021.168008.
[16] Antonov A, Gadetsky S, Granovsky A, Dyatckov A, Sedova M, Perov N, et al. High-frequency giant magneto-impedance in multilayered magnetic films. Physica A: Statical Mechanics and its Applications 1997;241:414–9. https://doi.org/10.1016/S0378-4371(97)00117-9.
[17] García C, Flores JM, Vargas P, Ross CA. Asymmetrical giant magnetoimpedance in exchange-biased NiFe. Appl Phys Lett 2010;96:232501. https://doi.org/10.1063/1.3446894.
[18] Vilela GLS, Monsalve JG, Rodrigues AR, Azevedo A, Machado FLA. Giant magnetoimpedance effect in a thin-film multilayer meander-like sensor. J Appl Phys 2017;121:124501. https://doi.org/10.1063/1.4978918.
[19] Mardani R. Fabrication of FM/NM/FM hetero-structure multilayers and investigation on structural and magnetic properties: application in GMI magnetic sensors. J Supercond Nov Magnetism 2020;33:503–9. https://doi.org/10.1007/s10948-019-05215-4.
[20] Kumar P, Rubi K, Mahendiran R. Room temperature giant magnetoimpedance in polycrystalline $La_{0.75}Ba_{0.25}MnO_3$. AIP Adv 2016;6:055913. https://doi.org/10.1063/1.4943244.
[21] Deb D, Debnath R, Mandal SK, Lakhani A, Nath A, Dey P. Effect of interface on temperature dependent magnetoresistance and room temperature magnetoimpedance of $La_{0.7}Sr_{0.3}MnO_3$/Polyvinyl Alcohol nanocomposites. Phys B Condens Matter 2020;582:411962. https://doi.org/10.1016/j.physb.2019.411962.
[22] Zhukov A, Ipatov M, Corte-León P, González-Legarreta L, Churyukanova M, Blanco JM, et al. Giant magnetoimpedance in rapidly quenched materials. J Alloys Compd 2020;814:152225. https://doi.org/10.1016/j.jallcom.2019.152225.
[23] Kraus L, Vazquez M, Knobel M. Giant magnetoimpedance. In: Buschow KHJ, editor. Handbook "magnetic materials", vol. 15. Amsterdam: North-Holland; 2003. p. 497–563. https://doi.org/10.1016/S1567-2719(03)15005-6.
[24] Nderu JN, Yamasaki J, Humphrey FB. Switching mechanism in Co based amorphous wire. J Appl Phys 1997;81:4036. https://doi.org/10.1063/1.364882.
[25] Tejedor M, Hernando B, Sánchez ML, Prida VM, Vázquez M. The torsional dependence of the magneto-impedance effect in current-annealed Co-rich amorphous wires. J Phys D: Appl Phys 1998;31:3331. https://doi.org/10.1088/0022-3727/31/23/005.
[26] Blanco JM, Zhukov A, Gonzalez J. Effect of tensile and torsion on GMI effect in amorphous wire. J Magn Magn Mater 1999;196–197:377–9. https://doi.org/10.1016/S0304-8853(98)00757-4. C. Garcia, A. Chizhik, A. Zhukov, V. Zhukova, J. Gonzalez, J.M. Blanco, L.V. Panina, "Influence of torsion and tensile stress on magnetoimpedance effect in Fe-rich amorphous microwires at high frequencies", J. Magn. Magn. Mater. 316, (2007) e896-e899; DOI: 10.1016/j.jmmm.2007.03.135.
[27] Dong J, Zhang Y, Zhang X, Zhao C, Liu Q, Wang J. Influence of tensile stress on giant magnetoimpedance effect of electroplated $Ni_{1-x}Co_x$/Cu composite wires. J Alloys Compd 2014;616:426–9. https://doi.org/10.1016/j.jallcom.2014.07.169.
[28] Alam J, Nematov M, Yudanov N, Podgornaya S, Panina L. High-frequency magnetoimpedance (MI) and stress-MI in amorphous microwires with different anisotropies. Nanomaterials 2021;11(5):1208. https://doi.org/10.3390/nano11051208.
[29] Usov NA, Antonov AS, Lagar'kov AN. Theory of giant magneto-impedance effect in amorphous wires with different types of magnetic anisotropy. J Magn Magn Mater 1998;185:159–73. https://doi.org/10.1016/S0304-8853(97)01148-7.
[30] Zhukova V, Blanco JM, Ipatov M, Churyukanova M, Taskaev S, Zhukov A. Tailoring of magnetoimpedance efect and magnetic softness of Fe-rich glass-coated microwires by stress- annealing. Sci Rep 2018;8:3202. https://doi.org/10.1038/s41598-018-21356-3.
[31] Kikuchi H, Urakawa Y, Tanii M. Changes in properties of thin-film magnetoimpedance element by Joule heating. J Magn Magn Mater 2021;539:168356. https://doi.org/10.1016/j.jmmm.2021.168356.
[32] Zhukov A, Gonzalez-Legarreta L, Corte-Leon P, Ipatov M, Blanco JM, Gonzalez J, et al. Tailoring of magnetic softness and magnetoimpedance of Co-rich microwires by stress-annealing. Phys Status Solidi 2021;218:2100130. https://doi.org/10.1002/pssa.202100130.
[33] Senda M, Ishii O, Koshimoto Y, Toshima T. Thin-film magnetic sensor using high frequency magneto-impedance (HFMI) effect. IEEE Trans Magn 1994;30:4611–3. https://doi.org/10.1109/20.334165.
[34] Panina LV, Mohri K, Uchiyama T, Noda M, Bushida K. Giant magneto-impedance in Co-rich amorphous wires and films. IEEE Trans Magn 1995;31:1249–60. https://doi.org/10.1109/20.364815.
[35] Uchiyama T, Mohri K, Jimbo M, Tsunashima S. Magnetoimpedance effect of CoSiB amorphous sputtered films. J. Magn. Soc. Japan. 1995;19:481–4.
[36] Ménard D, Britel M, Ciureanu P, Yelon A. Giant magnetoimpedance in a cylindrical conductor. J Appl Phys 1998;84:2805–14. https://doi.org/10.1063/1.368421.
[37] Aragoneses P, Zhukov A, Gonzalez J, Blanco JM, Dominguez L. Effect of AC driving current on Magneto-Impedance effect. Sensor Actuator 2000;81(1–3):86–90. https://doi.org/10.1016/S0924-4247(99)00092-8.

[38] Phan M-H, Peng H-X, Yu S-C, Vázquez M. Optimized giant magnetoimpedance effect in amorphous and nanocrystalline materials. J Appl Phys 2006;99:08C505. https://doi.org/10.1063/1.2162089.
[39] Chlenova AA, Moiseev AA, Derevyanko MS, Semirov AV, Lepalovsky VN, Kurlyandskaya GV. Permalloy-based thin film structures: magnetic properties and the giant magnetoimpedance effect in the temperature range important for biomedical applications. Sensors 2017;17:1900. https://doi.org/10.3390/s17081900.
[40] Yamadera H, Ohta N, Funabashi H. Micromachined thin film magnetoimpedance element for use in integrated magnetic sensors. R&D Review of Toyota CRDL 2014;45(2):35–40. https://www.tytlabs.com/review/issue/files/452_035yamadera.pdf.
[41] Gazda P, Szewczyk R. Novel giant magnetoimpedance magnetic field sensor. Sensors 2020;20(3):691. https://doi.org/10.3390/s20030691.
[42] Taysioglua AA, Peksoza A, Kayab Y, Derebasia N, Irezb G, Kaynak G. GMI effect in CuO coated Co-based amorphous ribbons. J Alloys Compd 2009;487:38–41. https://doi.org/10.1016/j.jallcom.2009.08.041.
[43] Laurita N, Chaturvedi A, Bauer Ch, Jayathilaka P, Leary A, Miller C, et al. Enhanced giant magnetoimpedance effect and field sensitivity in Co-coated soft ferromagnetic amorphous ribbons. J Appl Phys 2011;109:07C706. https://doi.org/10.1063/1.3548857.
[44] Han Y, Li X, Lv WX, Xie WH, Zhao Q, Zhao ZJ. Magnetoimpedance effect of FINEMET ribbons coated with $Fe_{20}Ni_{80}$ permalloy film. J Alloys Compd 2016;678:494–8. https://doi.org/10.1016/j.jallcom.2016.04.021.
[45] Eggers T, Lam DS, Thiagboh O, Marcin J, Svec P, Huong NT, et al. Impact of the transverse magnetocrystalline anisotropy of a Co coating layer on the magnetoimpedance response of FeNi-rich nanocrystalline ribbon. J Alloys Compd 2018;741:1105–11. https://doi.org/10.1016/j.jallcom.2018.01.206.
[46] Jamilpanah L, Hajiali MR, Mohseni SM, Erfanifam S, Mohseni SM, Houshiar M, et al. Magnetoimpedance exchange coupling in different magnetic strength thin layers electrodeposited on Co-based magnetic ribbons. J Phys D: Appl Phys 2017;50:155001. https://doi.org/10.1088/1361-6463/aa6098.
[47] Chen Y, Zou J, Shu X, Song Y, Zhao Z. Enhanced giant magneto-impedance effects in sandwich FINEMET/rGO/FeCo composite ribbons. Appl Surf Sci 2021;545:149021. https://doi.org/10.1016/j.apsusc.2021.149021.
[48] Volchkov SO, Pasynkova AA, Derevyanko MS, Bukreev DA, Kozlov NV, Svalov AV, et al. Magnetoimpedance of CoFeCrSiB ribbon-based sensitive element with FeNi covering: experiment and modeling. Sensors 2021;21(20):6728. https://doi.org/10.3390/s21206728.
[49] Zhukova V, Cobeño AF, Zhukov A, de Arellano Lopez AR, Blanco JM, Larin V, et al. Correlation between magnetic and mechanical properties of devitrified glass-coated Fe71.8Cu1Nb3.1Si15B9.1 microwires. J Magn Magn Mater 2002;249(I-II):79–84. https://doi.org/10.1016/S0304-8853(02)00509-7.
[50] Tejedor M, Hernando B, Sánchez ML, Prida VM, Vázquez M. The magnetostriction and stress dependence of the magneto-impedance effect in ribbons of amorphous $Fe_4Co_{67}Mo_{1.5}Si_{16.5}B_{11}$. J Phys D: Appl Phys 1998;31:2431. https://doi.org/10.1088/0022-3727/31/19/012.
[51] Herzer G. Anisotropies in soft magnetic nanocrystalline alloys. J Magn Magn Mater 2005;294:99–106. https://doi.org/10.1016/j.jmmm.2005.03.020.
[52] González-Legarreta L, Prida VM, Hernando B, Ipatov M, Zhukova V, Zhukov AP, et al. Magnetoimpedance dependence on width in $Co_{66.5}Fe_{3.5}Si_{12.0}B_{18.0}$ amorphous alloy ribbons. J Appl Phys 2013;114:053905. https://doi.org/10.1063/1.4790480.
[53] Talaat A, Ipatov M, Zhukova V, Zhukov AP, Gonzalez J, Gonzalez-Legarreta L, et al. High frequency magnetoimpedance response of stress annealed $Co_{66.3}Fe_{3.7}Si_{12.0}B_{18.0}$ amorphous alloy ribbons. J Appl Phys 2013;114:023904. https://doi.org/10.1063/1.4813101.
[54] Chizhik A, Vega V, Mohamed Abd El-Moez A, Prida VM, Sánchez T, Hernando B, et al. Surface magnetic properties and giant magnetoimpedance effect in Co-based amorphous ribbons. Intermetallics 2017;86:15–9. https://doi.org/10.1016/j.intermet.2017.03.010.
[55] Kurlyandskaya GV, Vázquez M, Muñoz JL, García D, McCord J. Effect of induced magnetic anisotropy and domain structure features on magnetoimpedance in stress annealed Co-rich amorphous ribbons. J Magn Magn Mater 1999;196–197:259–61. https://doi.org/10.1016/S0304-8853(98)00805-1.
[56] Ge J, Yang X, Wang S, Zhao J, Cheng M, He X, et al. Study of stress annealing effect on giant magneto-impedance of Fe-based ribbons. Emerg Mater Res 2016;5(1):62–6. https://doi.org/10.1680/jemmr.16.00004.
[57] Talaat A, Zhukova V, Ipatov M, Blanco JM, Gonzalez J, Zhukov A. Impact of stress annealing on the magnetization process of amorphous and nanocrystalline Co-based microwires. Materials 2019;12:2644. https://doi.org/10.3390/ma12162644.
[58] Tejedor M, Hernando B, Sanchez ML, Prida VM, Vázquez M. Magneto-impedance effect in amorphous ribbons for stress sensor application. Sensors & Actuators A: Physical 2000;81:98–101. https://doi.org/10.1016/S0924-4247(99)00095-3.
[59] Bensalah A-D, Barrué R, Alves F, Rached LA. Giant magneto-impedance sensors based on rapidly stress-annealed FeSiBCuNb ribbons. Sens Lett 2007;5(1):146–8. https://doi.org/10.1166/sl.2007.045.
[60] Wang T, Zhou Y, Lei C, Luo J, Xie S, Pu H. Magnetic impedance biosensor: a review. Biosens Bioelectron 2017;90:418–35. https://doi.org/10.1016/j.bios.2016.10.031.
[61] Zhao Y, Wang Y, Estevez D, Qin F, Wang H, Zheng X, et al. Novel broadband measurement technique on PCB cells for the field- and stress dependent impedance in ferromagnetic wires. Meas Sci Technol 2020;31:025901. https://doi.org/10.1088/1361-6501/ab4556.
[62] Guo LY, Wang X, Shen KC, Kim KB, Lan S, Wang XL, et al. Structure modification and recovery of amorphous $Fe_{73.5}Si_{13.5}B_9Nb_3Cu_1$ magnetic ribbons after autoclave treatment: SAXS and thermodynamic analysis. J Mater Sci & Technol 2019;35:118–26. https://doi.org/10.1016/j.jmst.2018.09.010.
[63] Karnaushenko D, Kang T, Schmidt OG. Shapeable material technologies for 3D self-assembly of mesoscale electronics. Adv. Mater. Technol. 2019;4:1800692. https://doi.org/10.1002/admt.201800692.
[64] Guo YB, Zou JT, Li X, Xie WH, Zhao ZJ. Magnetic properties and giant magnetoimpedance effect of FINEMET/$Fe_{50}Pt_{50}$ composite ribbons. J Magn Magn Mater 2020;513:167080. https://doi.org/10.1016/j.jmmm.2020.167080.
[65] Ipatov M, Zhukova V, Gonzalez J, Zhukov A. Magnetoimpedance sensitive to dc bias current in amorphous microwires. Appl Phys Lett 2010;97:252507. https://doi.org/10.1063/1.3529946.
[66] García C, Zhukova V, Ipatov M, González J, Blanco JM, Zhukov A. High-frequency GMI effect in glass-coated amorphous wires. J Alloys Compd 2009;488:9–12. https://doi.org/10.1016/j.jallcom.2008.05.110.
[67] Kraus L, Infante G, Frait Z, Vázquez M. Ferromagnetic resonance in microwires and nanowires. Phys Rev B 2011;83:174438. https://doi.org/10.1103/PhysRevB.83.174438.
[68] Zhukov A, Ipatov M, Talaat A, Blanco JM, Zhukova V. Studies of high frequency giant magnetoimpedance effect in Co-rich amorphous microwires. IEEE Trans Magn 2015;51(11):2003904. https://doi.org/10.1109/TMAG.2015.2436051.

[69] Barandiarán JM, Hernando A, Madurga V, Nielsen OV, Vázquez M, Vázquez-López MC. Temperature, stress and structural relaxation dependence of the magnetostriction in $(Co_{0.94}Fe_{0.06})_{75}Si_{15}B_{10}$ glasses. Phys Rev B 1987;35:5066–72. https://doi.org/10.1103/PhysRevB.35.5066.

[70] Siemko A, Lachowicz HK. On the origin of stress-dependent saturation magnetostriction in metallic glasses. J Magn Magn Mater 1990;89:21–5. https://doi.org/10.1016/0304-8853(90)90700-Z.

[71] Ipatov M, Zhukova V, González J, Zhukov A. Magnetoimpedance hysteresis in amorphous microwires induced by core-shell interaction. Appl Phys Lett 2014;105:122401. https://doi.org/10.1063/1.4896322.

[72] Zou J, Chen Y, Li X, Song Y, Zhao Z. Observation of the transition state of domain wall displacement and GMI effect of FINEMET/graphene composite ribbons. RSC Adv 2019;9:39133–42. https://doi.org/10.1039/C9RA07642E.

[73] Ipatov M, Zhukova V, González J, Zhukov A. Manipulating the magnetoimpedance by dc bias current in amorphous microwire. J Magn Magn Mater 2012;324:4078–83. https://doi.org/10.1016/j.jmmm.2012.07.024.

[74] Ipatov M, Zhukova V, Zhukov A, González J. Expanding the longitudinal magnetoimpedance sensor range by direct bias current. J Appl Phys 2013;113:203902. https://doi.org/10.1063/1.4807296.